RSC Advances

ROYAL SOCIETY OF CHEMISTRY

www.rsc.org/advances

Journal Name

COMMUNICATION

Effect of Mg^{2+}/Li^{+} mixed electrolytes on a rechargeable hybrid battery with $Li_4Ti_5O_{12}$ cathode and Mg anode

Received 00th January 20xx,
Accepted 00th January 20xx

DOI: 10.1039/x0xx00000x

www.rsc.org/

Qi Miao, Yanna NuLi,* Nan Wang, Jun Yang, Jiulin Wang and Shin-ichi Hirano

The rechargeable hybrid batteries with Li^+ insertion cathode, Mg anode and mixed Mg^{2+}/Li^+ electrolyte could synergistically exploit the advantages of Li^+ and magnesium. Herein, we report the electrolyte dependencies on the performance of a hybrid battery containing commercial $Li_4Ti_5O_{12}$ cathode. Additionally, the performance is improved using graphene based composite.

The rechargeable magnesium batteries have been proposed as a candidate of high energy density batteries for practical applications in electric vehicles and energy storage systems due to the inherent merits of metallic Mg such as natural abundance, high theoretical volumetric capacity (3832 mAh cm^{-3}) and operational safety.[1] Moreover, Mg can be considered as a safe anode in liquid electrolyte duo to non-dendritic deposits.[2] However, the development of Mg batteries suffers from electrolyte and the sluggish kinetics of Mg^{2+} ions in cathode originating from the strong coulombic interaction between bivalent Mg^{2+} and intercalation host.[3] A hybrid battery has been constructed combining Mg anode and Li^+-intercalation cathode in a mixed Mg^{2+}/Li^+ electrolyte to benefit from dendrite-free Mg and efficient Li^+ intercalation in terms of specific capacity, cycling stability, and rate capability.[4]

Herein, we report a hybrid Mg^{2+}/Li^+ battery, consisting of Mg anode, cheap and non-toxic commercial $Li_4Ti_5O_{12}$ (LTO) cathode, and two dual-salt electrolytes: 0.5 mol L^{-1} $Mg(BH_4)_2$+1.5 mol L^{-1} $LiBH_4$/tetraglyme (TG) (called $Mg(BH_4)_2$-based mixed electrolyte) or 0.4 mol L^{-1} $(PhMgCl)_2$-$AlCl_3$+1.5 mol L^{-1} $LiBH_4$/tetrahydrofuran (THF) (called APC-based mixed electrolyte). $Mg(BH_4)_2$-based mixed electrolyte is not corrosive towards stainless-steel current collector and casings (in contrast to both the "first generation" and "second generation" magnesium electrolytes and containing halogen Mg^{2+}/Li^+ mixed electrolytes).[5] The performance of $Mg(BH_4)_2$+$LiBH_4$/TG electrolytes with various $Mg(BH_4)_2$ and $LiBH_4$ concentrations has been systematically studied.[4d, 5] 0.5 mol L^{-1} $Mg(BH_4)_2$+1.5 mol L^{-1} $LiBH_4$/TG shows the highest current density and efficiency for Mg deposition-dissolution, and higher capacities and better cycling performance using as the electrolyte for TiO_2/Mg coin. Herein, the same concentration $LiBH_4$ was added in "second generation" magnesium electrolyte 0.4 mol L^{-1} $(PhMgCl)_2$-$AlCl_3$/THF as another dual-salt electrolyte. The effect of dual-salt electrolytes on the electrochemical performance of LTO|Mg cells was studied. Spinel LTO is an excellent Li^+-insertion material due to the unique feature of zero-strain during lithium intercalation/deintercalation.[6] Furthermore, LTO has an appropriate lithiation voltage plateau at 1.54 V versus Li/Li^+, within the electrochemical stability window of the magnesium electrolyte when non-inert metals are used as the current collector. However, LTO has pretty low electronic conductivity (ca. 10^{-13} S cm^{-1}) and moderate Li^+ diffusion coefficient (10^{-9}-10^{-13} cm^2 s^{-1}).[7] Additionally, LTO/G composite prepared by simply ball-milling LTO with graphene (G), which has large surface area, excellent electronic and thermal conductivity, and high mechanical strength,[8] was used as cathode material, which delivers higher specific capacity, and better cycling life and rate capability. This work demonstrates the importance of compatibility of the cathode materials and electrolytes in rechargeable hybrid batteries.

Commercially available LTO (Shenzhen Tianjiao Technology Co., Ltd.) was used without further treatment. LTO/G composite was prepared by simple ball-milling LTO with graphene powder (Deyang Carbonene Technology Co., Ltd.) at different weight ratios of 80:20, 70:30 and 60:40. The discharge-charge cycling result (Fig. S1a, Table S1) shows a high content of graphene improves the first discharge capacity. However, the initial coulombic efficiency increases over 100 %, which is resulted from some side reaction (discussed below). The phenomenon becomes more severe with the increase of graphene content duo to increased surface area of the composite. More graphene also influences the uniform dispersion of LTO particle in the composite as shown in SEM images of Fig. S1b, thus results in poor cycling performance. 20 wt.% of added graphene in LTO can provide an improved electrochemical performance with an acceptable coulombic efficiency and better cycling performance.

The corresponding X-ray diffraction (XRD) pattern, Raman, and scanning and transmission electron microscope (SEM and TEM) images are presented in Fig. 1. The diffraction peaks shown in Fig. 1a can be indexed to $Li_4Ti_5O_{12}$ with JCPDS No. 49-0207 (space group:

School of Chemistry and Chemical Engineering, Shanghai Electrochemical Energy Devices Research Center, Hirano Institute for Materials Innovation, Shanghai Jiao Tong University, Shanghai 200240, PR China. Fax: (+86) 21-5474-1297; Tel: (+86) 21-5474-5887; E-mail: nlyn@sjtu.edu.cn

Electronic Supplementary Information (ESI) available: [details of any supplementary information available should be included here]. See DOI: 10.1039/x0xx00000x

Fd$\bar{3}$*m*). The sharp and strong diffraction peaks of LTO indicate a well-defined crystal structure. XRD pattern of LTO/G (80:20) exhibit little change, which is mainly because of the low amount of graphene within the composite. Raman spectroscopy is a powerful analytical tool for carbon materials to evaluate the degree of graphitic order. As shown in Fig. 1b, graphene powder and LTO/G sample both show two main peaks corresponding to G and D bands, which is due to the in-plane stretching vibration (E_{2g}) of the sp^2-bonded carbon atoms and symmetrical breathing vibration (A_{1g}) of the hexagonal carbon rings, respectively. [9] The intensity ratio between D and G band, (I_D/I_G) is usually used to measure the defect density in the carbon nanostructures. The increased I_D/I_G ratio for LTO/G sample is ascribed to an enhanced structural distortion caused by LTO within the graphene sheets, as shown in Fig. 1d. The particles (Fig. 1c) are found to be a few micrometers in size, and decrease a little after mill-balling (Fig. 1d). SEM image of LTO/G shows the coexistence of the particle-like LTO and wrinkled layered graphene sheets, and these wrinkles are the indication of highly defective morphology of the structure. The distribution of LTO particles over graphene is illustrated by TEM images (Fig. 1f).

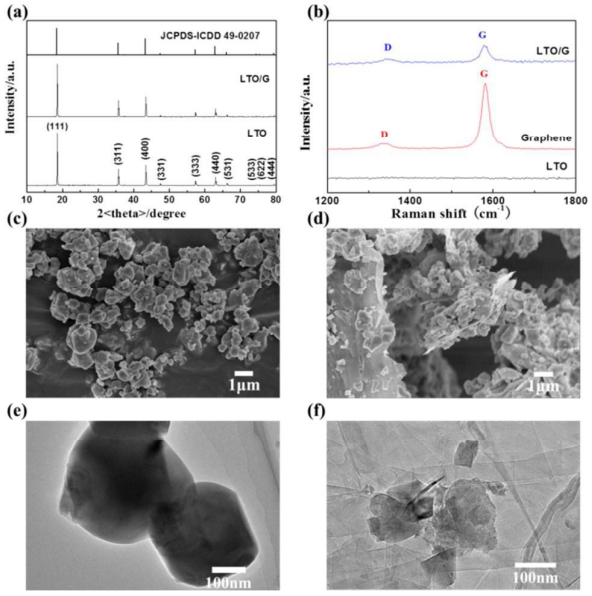

Figure 1. (a) X-ray diffraction pattern of LTO and LTO/G (80:20) composite and the standard pattern of LTO. (b) Raman spectrum of LTO, graphene and LTO/G (80:20) composite. SEM images of LTO (c) and LTO/G composite (d). TEM images of LTO (e) and LTO/G composite (80:20) (f).

Fig. 2a shows first galvanostatic discharge/charge curves of LTO cathode in three different cells: LTO|0.5 mol L^{-1} $Mg(BH_4)_2$/TG|Mg, LTO|1.5 mol L^{-1} $LiBH_4$/TG|Li and LTO|0.5 mol L^{-1} $Mg(BH_4)_2$+1.5 mol L^{-1} $LiBH_4$/TG|Mg at a rate of 0.1 C (1 C = 175 mA g^{-1}). LTO barely delivers any capacity in the LTO|Mg^{2+}|Mg cell, indicating that Mg^{2+} could not intercalate into LTO structure. It has been reported that magnesium storage behaviors in LTO are strongly size dependent and Mg^{2+} electrochemical insertion into LTO are notable only when the particle size is below 40 nm. [10] On the contrary, the behavior of LTO|Li^+|Li cell is typical of LTO in a lithium electrolyte with a flat plateau at an average potential of 1.55 V which is attributed to a two-phase phenomenon pertaining to $Li_4Ti_5O_{12}$ and $Li_7Ti_5O_{12}$ phases. [11] In the LTO|Li^+, Mg^{2+}|Mg cell, similar discharge/charge curves and a comparable capacity with higher polarization as that in the LTO|Li^+|Li cell are shown, indicating similar reaction in the hybrid cell. The higher polarization is likely resulted from the lower electronic conductivity of the dual salt electrolyte than lithium electrolyte (616 and 634 μS cm^{-1}, respectively).

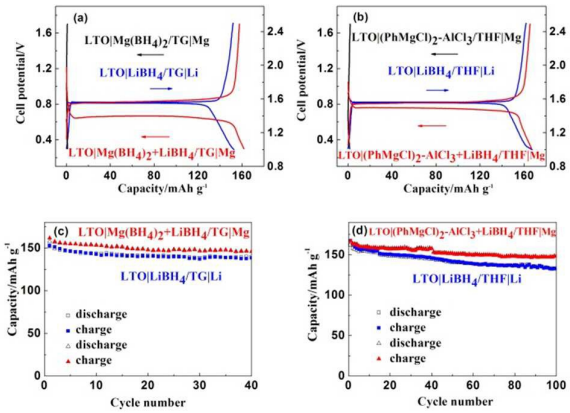

Figure 2. Discharge-charge profiles of (a) LTO|$Mg(BH_4)_2$/TG|Mg, LTO|$LiBH_4$/TG|Li and LTO|$Mg(BH_4)_2$+$LiBH_4$/TG|Mg cells, and (b) LTO|$(PhMgCl)_2$-$AlCl_3$/THF|Mg, LTO|$LiBH_4$/THF|Li and LTO|$(PhMgCl)_2$-$AlCl_3$+$LiBH_4$/THF|Mg at 0.1 C. (c) (d) Cycling performance of LTO|Li cells with lithium electrolytes and LTO|Mg cells with mixed electrolytes at 0.1C.

Considering the possible influence of electrolytes on the electrochemical performance, the performance of the cells with APC-based mixed electrolyte was further tested. Fig. 2b shows the first galvanostatic discharge/charge curves of LTO cathode in three cells: LTO|0.4 mol L^{-1} $(PhMgCl)_2$-$AlCl_3$/THF|Mg, LTO|1.5 mol L^{-1} $LiBH_4$/THF|Li and LTO|0.4 mol L^{-1} $(PhMgCl)_2$-$AlCl_3$+1.5 mol L^{-1} $LiBH_4$/THF|Mg at a rate of 0.1 C. Similarly, LTO|Mg^{2+}|Mg cell delivers little capacity, and LTO|Li^+, Mg^{2+}|Mg shows comparable capacity with higher voltage polarization than LTO|Li^+|Li cell. However, the APC-based mixed electrolyte has higher electronic conductivity than the lithium electrolyte (3.18 mS cm^{-1} and 853 μS cm^{-1}, respectively). It is suggested that higher voltage polarization is mainly related to higher overpotential of Mg deposition-dissolution than that of Li deposition-dissolution (Fig. S2a). Notably, the cell with APC-based mixed electrolyte presents lower voltage polarization than that with $Mg(BH_4)_2$-based mixed electrolyte. Fig. 2c and 2d displays the discharge and charge capacities with respect to cycle number at 0.1 C of LTO|Li^+, Mg^{2+}|Mg cells with $Mg(BH_4)_2$-based and APC-based mixed electrolytes. As a comparison, the LTO|Li^+|Li cells with lithium electrolytes are also represented. Partly due to higher and more stable deposition-dissolution efficiencies of Mg than Li (Fig. S2b), the hybrid cells show better cycling performance than lithium cells (92.6% and 91.8% capacity retention for $Mg(BH_4)_2$+$LiBH_4$/TG and $LiBH_4$/TG, respectively), especially with APC-based mixed electrolyte (95.3% and 89.4% for $(PhMgCl)_2$-$AlCl_3$+$LiBH_4$/THF and $LiBH_4$/THF, respectively). The reversible specific capacities of hybrid battery with $(PhMgCl)_2$-$AlCl_3$+$LiBH_4$/THF electrolyte remain at the quite considerable value of ~160 mAh g^{-1} for all of the cycles. For LTO|Li^+, Mg^{2+}|Mg cells, over 100 % coulombic efficiency during discharging/charging appears in two mixed electrolytes (Fig. S3), which is resulted from

electrolyte and/or PVDF decomposition during charging (Fig. S4). Both of mixed electrolytes have approximate 2.5 V anodic stability on stainless steel (SS), however, the values decrease notably when introducing binder, which is a necessary component for powder electrode. To examine the PVDF decomposition, the 70% PVDF+30% Super-P electrodes were scanned by the liner sweep voltammetry to different cut-off potentials, after which the amounts of carbon and fluorine were compared (Table S2). C and F amounts change linearly with the increase of cut-off potentials, indicating the bonds in PVDF might be in part loosen or broken during the oxidation process. LTO undergoes more decomposition in APC-based mixed electrolyte duo to the lower anodic stability. However, APC-based mixed electrolyte shows higher electronic conductivity (3.18 ms cm^{-1} and 616 μs cm^{-1}, respectively), higher cycling efficiencies and lower overpotential for Mg deposition-dissolution (Fig. S5) than $Mg(BH_4)_2$-based mixed electrolyte, which is contributed to the better performance.

Cyclic voltammetry (CV) was used to further investigate the electrochemical behavior of LTO|Li^+, Mg^{2+}|Mg with APC-based mixed electrolyte at different scan rates. As shown in Fig. 3a, only one pair of prominent cathodic/anodic peaks can be observed. The actual peak potentials depend on the scan rate, and the reversibility increases with decreasing scan rate. The cathodic (intercalation) and anodic (de-intercalation) peaks are in accordance with the plateaus of the discharging/charging curves. The main redox reaction corresponds to $Li_4Ti_5O_{12}/Li_7Ti_5O_{12}$ conversion, which are also assigned to the flat voltage platforms in the discharging and charging curves. In order to study the acceleration of graphene to the reversibility of the intercalation process, CV of LTO/G (80:20)|Li^+, Mg^{2+}|Mg with same electrolyte at 0.01 mV s^{-1} was carried out (Fig. 3b). Compared with those of LTO, the intensities of cathodic/anodic peaks increase and voltage difference of the peaks for LTO/G decrease, indicating a lower polarization and better reversible intercalation and de-intercalation of Li^+. To gain further understanding on the improved electrochemical performance, electrochemical impendence spectra (EIS) measurements were employed to characterize the cells with LTO and LTO/G (80:20) cathodes after CV measurements. As shown in Fig. 3c, both of the Nyquist plots are composed of a depressed semicircle at high-to-medium frequency and a long inclined line at low frequency. The semicircle corresponds to the charge transfer process at the interface between the electrolyte and electrode, and the linear segment relates to the ion diffusion within the cathode. The impedance spectra were fitted with a model circuit (inset of Fig. 3c), where R_s is the resistance of the electrolyte, and R_{ct} is the charge-transfer resistance at the electrode/electrolyte interface. Z_W is the diffusive Warburg impedance. A constant phase element, abbreviated to CPE, is placed to represent the double-layer capacitance due to the surface roughness of the particle.[12] The fitted resistance values from EIS are displayed in Table S2. R_{ct} value for LTO/G electrode is smaller than that of the LTO electrode, thus demonstrating the lower charge-transfer resistance. The major contribution is attributed to the higher specific surface area of the graphene framework, which facilitates fast electron transport from the poorly conducting LTO by their close contact. Furthermore, it can be observed that the slope corresponding to Warburg impedance is greater for the LTO/G composite than that of LTO, meaning that the ion transport process within the LTO/G electrode is also improved. As a result, the LTO/G (80:20) composite shows higher specific capacities and better cycling stability than LTO at 0.1 C (97.3% and 94.0%, respectively) and 0.15 C (90.6% and 86.2%, respectively), as shown in Fig. S1a and Fig. 3d.

To further discuss the effect of graphene on the performance, discharge-charge cycling test of LTO/G|Li^+, Mg^{2+}|Mg hybrid cell with APC-based electrolyte at 0.2 C was carried out and the initial three discharge-charge profiles are shown in Fig. 3e. The voltage polarization decreases and the specific capacities increase compared with LTO|Li^+, Mg^{2+}|Mg cell. Fig. 3f further presents the comparison of the capacities at various current rates from 0.2 to 2 C for LTO/G|Li^+, Mg^{2+}|Mg and LTO|Li^+, Mg^{2+}|Mg cells with APC-based electrolyte. The LTO/G electrode shows higher reversible capacity, better cyclability, especially at high current densities. At the rates from 0.2 to 2 C, the discharge and charge capacities match each other well during cycling. At a relatively low rate of 0.2 C, LTO/G exhibits an initial discharge capacity of 152 mAh g^{-1} and charge capacity of 150.9 mAh g^{-1}. The discharge capacity at 0.4 C, 1 C and 2 C is 132.9, 90.1 and 55.7 mAh g^{-1}, respectively. In addition, a capacity of ~135 mAh g^{-1} and 145 mAh g^{-1} at 0.2 and 0.1 C, respectively, is retained after discharge/charge cycles at various preceding rates, indicating the relatively high rate performance than LTO due to the better electronic conductivity.

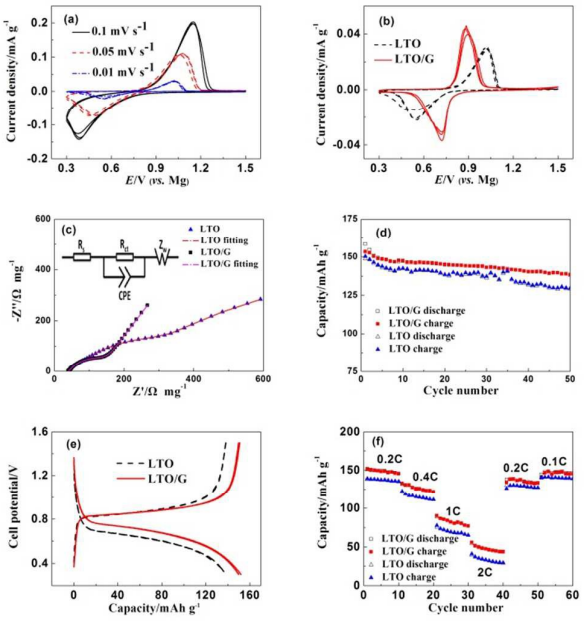

Figure 3. CVs of the cells (a) LTO|Li^+, Mg^{2+}|Mg at different scan rates, (b) LTO and LTO/G (80:20)|Li^+, Mg^{2+}|Mg at 0.01 mV S^{-1}, and (c) the Nyquist plots of the cells after CV measurements, inset is the model circuit. (d) The cycling performance of LTO and LTO/G (80:20)|Li^+, Mg^{2+}|Mg cells at 0.15 C. (e) The initial three discharge-charge profile of LTO and LTO/G (80:20)|Li^+, Mg^{2+}|Mg cells at 0.2 C. (f) Rate capability of LTO and LTO/G (80:20)|Li^+, Mg^{2+}|Mg cells. The electrolyte is 0.4 mol L^{-1} $(PhMgCl)_2$-$AlCl_3$+1.5 mol L^{-1} $LiBH_4$/THF.

It is known that the morphology variation of electrode in cycling shows close relationship with the electrochemical performance. For further understanding the cause of the better performance of LTO/G than LTO, the morphology of the electrodes after rate cycles was compared. As shown in Fig. S6a, some cracks are present in the LTO electrode. The cracks would result in electrical isolation of active material particles and be responsible for the performance degradation of the testing cells. In comparison, LTO/G electrode does not exhibit such cracks, as seen in Fig. S6b. This is most likely due to the mechanical strength and resilience of the graphene helping to connect the active particles as well as

maintain good electronic contact of particles during cycling. The enhanced rate performance is more obvious in $Mg(BH_4)_2$-based mixed electrolyte with lower electronic conductivity (Fig. S7).

In summary, we investigated the effect of electrolytes on the electrochemical performance of a hybrid battery with commercial LTO cathode, Mg anode, and $Mg(BH_4)_2$-based or APC-based mixed electrolytes. By properly tuning electrolyte, commercial LTO shows good cycle stability. In addition, in this Li^+ insertion material, graphene emerges as an effective parameter in enhancing the capacities and rate performance. This work can be expected to have impact on the study of compatibility of cathode with electrolyte in hybrid Mg^{2+}-Li^+ batteries, which is of practical relevance for the development of batteries with metal Mg anode.

Financial support from the National Natural Science Foundation of China (No. 21273147, 21573146) and the Shanghai Municipal Science and Technology Commission (Project No. 11JC1405700) is gratefully acknowledged.

Notes and references

1 a) D. Aurbach, Z. Lu, A. Schechter, Y. Gofer, H. Gizbar, R. Turgeman, Y. Cohen, M. Moshkovich, E. Levi, *Nature*, 2000, **407**, 724; b) J. Muldoon, C.B. Bucur, A.G. Oliver, T. Sugimoto, M. Matsui, H.S. Kim, G.D. Allred, J. Zajicek, Y. Kotani, *Energy Environ*. *Sci.*, 2012, **5**, 5941.

2 M. Matsui, *J. Power Sources*, 2011, **196**, 7048.

3 a) H.S. Kim, T.S. Arthur, G.D. Allred, J. Zajicek, J.G. Newman, A.E. Rodnyansky, A.G. Oliver, W.C. Boggess, J. Muldoon, *Nat. Commun*., 2011, **2**, 427; b) P. Novák, J. Desilvestro, *J. Electrochem. Soc.*, 1993, **140**, 140.

4 a) T. Gao, F. D. Han, Y. J. Zhu, L. M. Suo, C. Luo, K. Xu, C. S. Wang, *Adv. Energy Mater.*, 2014, **5**, 1401507; b) Y. W. Cheng, Y. Y Shao, J. G. Zhang, V. L. Sprenkle, J. Liu, G. S. Li, *Chem. Commun.* 2014, **50**, 9644; c) S. Yagi, T. Ichitsubo, Y. Shirai, S. Yanai, T. Doi, K. Murase, E. Matsubara, *J. Mater. Chem. A*, 2014, **2**, 1144; d) S. J. Su, Z. G. Huang, Y. N. NuLi, F. Tuerxun, J. Yang, J. L. Wang, *Chem. Commun.*, 2015, **51**, 264; e) N. Wu, Z.-Z. Yang, H.-R. Yao, Y.X. Yin, L. Gu, Y.-G. Guo, *Angew. Chem., Int. Ed.*, 2015**, 54**, 5757; f) H. D. Yoo, Y. L. Liang, Y. F. Li, Y. Yao, *ACS Appl. Mater. Interfaces*, 2015, **7**, 7001.

5 F. Tuerxun, Y. Abulizi, Y. N. NuLi, S. J. Su, J. Yang, J. L. Wang, *J. Power Sources*, 2015, **276**, 255.

6 L. Zhao, Y-S. Hu, H. Li, Z. X. Wang, L. Q. Chen, *Adv. Mater*., 2011, **23**, 1385.

7 a) C. Y. Ouyang, Z. Y. Zhong, M. S. Lei, *Electrochem. Commun*., 2007, **9**, 1107; b) C. H. Chen, J. T. Vaughey, A. N. Jansen, D. W. Dees, A. J. Kahaian, T. Goacher, M. M. Thackeray, *J. Electrochem. Soc*., 2001, **148**, A102; c) M. Wagemaker, E. R. H. van Eck, A. P. M. Kentgens, F. M. Mulder, *J. Phys. Chem. B*, 2009, **113**, 224; d) Y. H. Rho, K. Kanamura, *J. Solid State Chem*., 2004, **177**, 2094.

8 a) Y. Sun, Q. Wu, G. Shi, *Energy Environ*. *Sci.*, 2011, **4**, 1113; b) J. Hou, Y. Shao, M. W. Ellis, R. B. Moore, B. Yi, Phys. Chem. Chem. Phys., 2011, **13**, 15384; c) B. P. Vinayan, N. I. Schwarzburger and M. Fichtner, *J. Mater. Chem. A*, 2015, **3**, 6810.

9 a) Z. M. Zhang, Q. Wang, C. J. Zhao, S. D. Min, X. Z. Qian, *ACS Appl. Mater. Interfaces*, 2015, **7**, 4861; b) M. Mowry, D. Palaniuk, C. C. Luhrs, S. Osswald, *RSC Adv*., 2013, **3**, 21763; c) A. C. Ferrari, *Solid State Commun*., 2007, **143**, 47.

10 a) N. Wu, Y.X. Yin, Y.G. Guo, *Chem. Asian J.* 2014, **9**, 2099; b) N. Wu, Y.C. Lyu, R.J. Xiao, X.Q. Yu, Y.X. Yin, X.Q. Yang, H. Li, L. Gu, Y.G. Guo, *NPG Asia Materials* 2014, **6**, e120.

11 A. S. Prakash, P. Manikandan, K. Pamesha, M. Sathiya, J-M. Tarascon, A. K. Shukla, *Chem. Mater*. 2010, *22*, 2857.

12 K. Dokko, M. Mohamedi, M. Umeda, I. Uchida, *J. Electrochem. Soc*. 2003, **150**, A425.

Effect of Mg^{2+}/Li^{+} mixed electrolytes on a rechargeable hybrid battery with $Li_4Ti_5O_{12}$ cathode and Mg anode

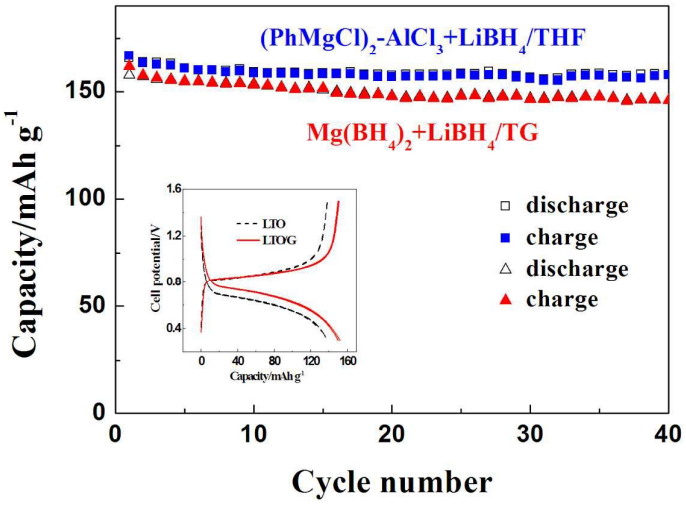

The electrolytes affect the electrochemical performance of a hybrid battery with commercial LTO cathode, Mg anode, and $Mg(BH_4)_2$-based or APC-based mixed Mg^{2+}/Li^{+} electrolytes. LTO shows better cycle stability in $Mg(BH_4)_2$-based mixed electrolyte, demonstrating the importance of compatibility of the cathode materials and electrolytes in rechargeable hybrid batteries. In addition, graphene emerges as an effective parameter in enhancing the capacities and rate performance of LTO.